Hydration development and thermal performance of calcium sulphoaluminate cements containing microencapsulated phase change materials

Susana G. Sanfelix[a,b], *Jesus D. Zea-García*[b], *Diana Londono-Zuluaga*[b$], *Isabel Santacruz*[b], *Angeles G. De la Torre*[b], *Anna-Lena Kjøniksen*[a*]

[a] Faculty of Engineering, Østfold University College, P.O. Box 700, N-1757 Halden, Norway

[b] Departamento de Química Inorgánica, Cristalografía y Mineralogía, Universidad de Malaga, Campus Teatinos s/n., 29071 Málaga, Spain

[$]Currently in: Laboratory of Construction Materials (LMC), EPFL STI IMX LMC Station 12, 1015 Lausanne, Switzerland

ABSTRACT

Microencapsulated phase change materials (MPCM) incorporated in buildings walls can reduce indoor temperature fluctuations, conserving energy and enhancing thermal comfort. MPCM were incorporated in calcium sulphoaluminate cement (CSA) at high concentrations to achieve a significant effect on the thermal properties. The cement hydration development was studied by isothermal calorimetry and laboratory X-Ray powder diffraction (LXRPD). The hydration mechanism was not affected by the addition of MPCM. In order to obtain homogeneous mortars in the presence of MPCM, a superplasticizer (SP) was used. However, the SP causes a significant delay of the hydration. Although the mineralogical composition of the hydrated pastes did not change with the addition of MPCM, the mechanical strengths decrease dramatically. This decrease is well described by the Bolomey equation, assuming MPCMs act as air voids. This is a physical effect due to the high volume of MPCM, and not due to a change in the hydration chemistry.

KEYWORDS

Phase Change Materials; Calcium Sulphoaluminate Cement; XRD Quantification; Cement Hydration

1. INTRODUCTION

Calcium sulphoaluminate cements (CSA) are considered low CO_2 emission materials [1]. The main constituent of the clinker is ye'elimite ($C_4A_3\bar{S}$) in combination with other phases such as belite, gehlenite and calcium aluminates. In order to obtain an optimum setting time, strength development, and volume stability, the clinker is ground with 10-25 wt% calcium sulphate (usually anhydrite). The resulting hydration phases depend on the amount and reactivity of the interground calcium sulphate, of which the main ones are ettringite, monosulphate, aluminum hydroxide as well as strätlingite or C-S-H (calcium silicate hydrates) [2-7]. In recent years, CSA cements have been evaluated as seasonal thermal storage materials, since their main hydrated compound is ettringite, a mineralogical phase with a high number of water molecules in its structure [8-10]. However, some of the drawbacks of using ettringite for thermal energy storage is a lack of stability, and crack formation. In addition, it is difficult to achieve an optimal charging and discharging of the reversible energy storage.

Incorporation of microencapsulated phase change materials (MPCM) in building materials is a promising solution in building construction. MPCM contribute to reduce the energy consumption [11-13], and provide thermal comfort of buildings. In order to introduce MPCM in sustainable construction, several combinations between MPCM and building materials can be used [14]. MPCMs are classified in three main families: organic, inorganic and eutectic [15, 16].

Several studies are related to addition of MPCM to plaster [17], geopolymers [18-20] or Portland cement (PC) composites [21]. Even though the cement industry is focused on decreasing the use of Portland cement because of its high CO_2 emissions, the majority of the literature regarding introducing MPCM in the cement matrix is utilizing on Portland cement [22]. Although there are a few exceptions, such as magnesium phosphate cements [23].

However, studies related to how CSA cement interacts with MPCM are still lacking. A recent study is related to sulphoaluminate cement composites combining steel fibers and PCM [24]. Evaluation of the hydration development of cement mortar and how MPCM can affect the hydration kinetics has been reported [25]. However, there is no available literature regarding the way the different hydrated phases of the cement can interact with MPCM or how polycarboxylate ether superplasticizers (SP) (commonly used to improve workability of MPCM composites) can interact with MPCM and the cement matrix.

In this study, we aim to elucidate whether organic paraffin based MPCM can affect or be affected by the CSA cement matrix. The study is conducted using isothermal calorimetry to evaluate hydration kinetics as well as hydration degree, and by Rietveld quantitative study to evaluate if the different hydrated phases are being affected by MPCM. It is already known that pure MPCM can be degraded in a gypsum environment [21]. In addition, the thermal properties of the cement composites are evaluated by DSC (differential scanning calorimetry) and TGA (thermogravimetric analysis) in order to evaluate their stability during the hydration processes. Finally, the porosity of the cement composites was determined by MIP (mercury intrusion porosimetry), and the compressive strength of standard mortar was examined.

2. EXPERIMENTAL SECTION

2.1 Materials, compositions and sample preparation

A MPCM powder, MPCM24D (Mikrotek Laboratories Inc.) was used in this study. It is a microencapsulated paraffin: 85-90% PCM and 10-15% polymeric shell (melamine-formaldehyde) [26]. This MPCM was selected due to its price, good references based on previous papers [27] and its hydrophilic shell which is more compatible with the cement paste [28]. The thermal properties of MPCM D24 are shown in Table 1.

Table 1. Thermal properties of the MPCM used in this study

MPCM	Product type	Melting				Freezing			
		Onset (ºC)	Endset (ºC)	Peak (ºC)	Enthalpy (J/g)	Onset (ºC)	Endset (ºC)	Peak (ºC)	Enthalpy (J/g)
Microtek®D24	Powder	16.6	26.6	23.7	119.1	22.3	15.1	19.2	120.3

CSA cement was prepared by mixing 75 wt% of a CSA-clinker (manufactured in China and marketed in Europe by BELITH S.P.R.L Belgium) with 25 wt% of anhydrite. Anhydrite was obtained by calcining a commercial bassanite from BELITH S.P.R.L. (Belgium) at 700°C for 60 min [29]. Chemical and mineralogical compositions are presented in Table 2. The relatively high ACn content is caused by the lower clinkering temperature and higher aluminate content of CSA compared to Portland cement, and is in agreement with previous studies of CSA [30, 31].

Table 2. Chemical composition (expressed as wt% of oxides) and mineralogical phase assemblage (determined by Rietveld method including amorphous and crystalline non-quantified, ACn, by internal standard method), in weight percentage (wt%) of the materials used in this study.

	CSA clinker	**Anhydrite**		**CSA-cement**	**Anhydrite**
CaO	41.97	40.61	**C_2S**	14.4	-
SiO_2	8.2	0.89	**$C_4A_3\overline{S}$**	36.6	-
Al_2O_3	33.8		**$C\overline{S}$**	23.6	99.1(1)
Fe_2O_3	2.37	0.06	**CT**	2.3	-
MgO	2.73	0.33	**Akermanite**	0.6	-
SO_3	8.8	56.71	**Mayenite**	1.8	-
K_2O		0.01	**SiO_2 (Quartz)**		0.4(1)
Na_2O	<0.08	0.15	**$CaCO_3$**		0.5(1)
Eq.Na_2O					
Cl		0.006			

LoI	0.75	**ACn**	20.7	

The chemical composition was measured by X-ray fluorescence (XRF) and the mineralogical composition was determined by XRD (X-ray diffraction) and the Rietveld method [32, 33] jointly with the internal standard methodology as detailed below. Figure 1 gives the particle size distribution of CSA cement and MPCM D24 measured by laser diffraction with a Malvern Mastersizer 2000, using a dry chamber.

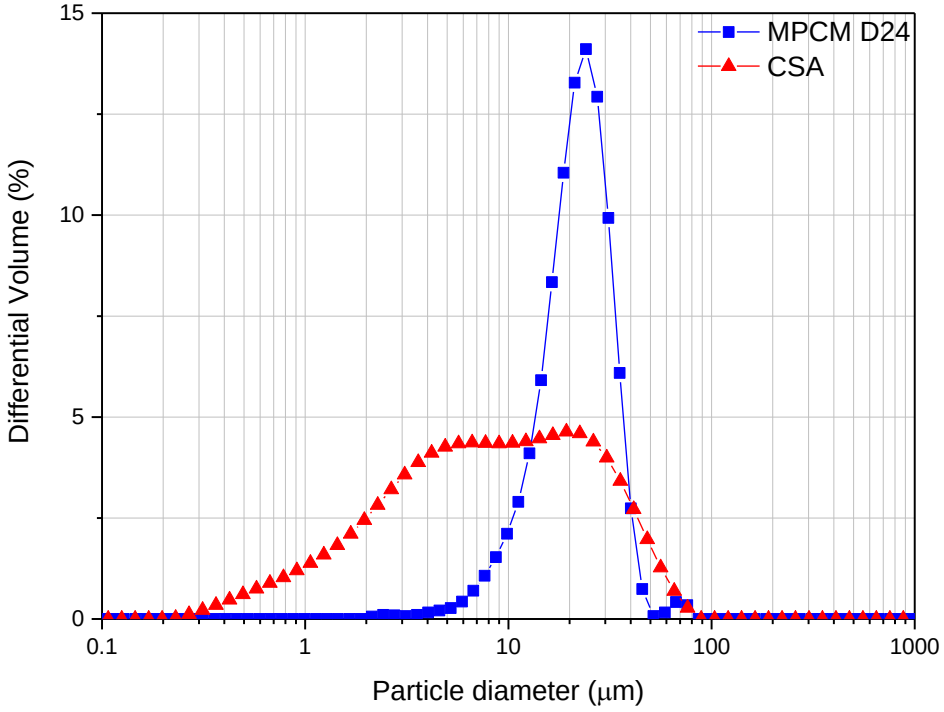

Figure 1. Particle size distribution of the CSA cement and MPCM D24

Cementitious samples were further studied without and with MPCM. Based on results from a previous study [28], the amount of MPCM D24 was set to 45 wt% with respect to dry cement, with the objective to have a composite material with good thermal properties. Pastes were prepared using mechanical stirring, as described previously [34]. Mixing proportions are given in Table 3.

Solid powders were first dry mixed, then deionized water was added at the w/c ratio given in Table 3. Superplasticizer, SP, (KHEMEFLOW 1030, Kheme chemicals S.A., which contains 35 wt% of active matter) was used in the pastes with MPCM to improve the fluidity of the mixtures. The SP was utilized at a concentration of 2.0 wt %, where all particles are coated by the admixture (determined by rheological measurements) [28, 35].

Cementitious pastes were cast in a Teflon mold with eight cylinders (1 cm diameter) and filled with cement paste [7]. The device was sealed and introduced in a humidity chamber at 95% RH at 20ºC. The device was rotating during the first 24 hours, in order to obtain homogeneous samples. After each curing time (1, 7, 28 and 56 days), two different steps were conducted depending on sample type.

Table 3. Mixing proportions (in weight percentage) and w/c ratios of the cement pastes.

Sample	w/c	w/s	Cement (wt%)	Water (wt%)	SP (wt% with respect to solids content)	MPCM D24 (wt%)
CSA-control	0.50	0.5	66.7	33.3	-	-
CSA-D24	0.50	0.3	50.5	25.3	2	22.7
CSA-control-075	0.75	0.75	57.1	42.9	-	-
CSA-D24-075	0.75	0.65	45.5	34.1	-	20.5

2.2 Analytical methods

2.2.1. Differential Thermal Analysis - Thermogravimetric Analysis (DTA-TGA)

DTA-TGA measurements were performed by a SDT-Q600 analyzer from TA Instruments (New Castle, DE). The temperature was varied from room temperature to 1000°C at a heating rate of 10 °C/min. Measurements were carried out in open platinum crucibles under air flow. The equipment

is composed with an electronic ultra-microbalance with a resolution of 0.1 µg and a maximum capacity of 200 mg, temperature sensors, a computer and a furnace equipped with an electrical resistance (max. temp. 1500ºC). The acquisition of the data was conducted by means of TA Universal Analysis software. The hydration of control samples was stopped prior to these measurements with acetone and ether [36]. Contrarily, samples with MPCM were measured without stopping the hydration, as these samples could not be stopped by chemical treatment, since the organic solvent may penetrate the shell of the MPCM and dissolve the paraffin in the core of the microcapsules.

2.2.2. Isothermal Calorimetry

Isothermal calorimetry was performed in an eight-channel Thermal Activity Monitor (TAM Air, TA Instruments) instrument using glass ampoules. Pastes were prepared *ex-situ* by mixing ~6 g of each sample with the appropriate amount of water, followed by manually stirring for 1 minute, and were thereafter immediately introduced in the calorimeter. A stabilization period of 45 min was needed prior to the start of the measurements. The heat production rate (thermal power, mW/g cement) and the heat (integral of thermal power, J/g cement) [37] were collected for up to 7 days at 20°C.

2.2.3. Laboratory X-Ray Powder Diffraction (LXRPD) data collection

LXRPD was performed in a D8 ADVANCE DaVinci diffractometer (Bruker AXS, Germany) (250 mm radius) with a Molybdenum X-Ray tube, a primary Johansson monochromator Ge (111), which gives a strictly monochromatic radiation ($\lambda = 0.7093$ Å), MoKα_1, and in transmission mode. The X-ray tube worked at 50 kV and 50 mA. The optics configuration was a fixed divergence slit (2°) and a fixed diffracted anti-scatter slit (9°) and the energy-dispersive linear detector

LYNXEYE XE 500 μm, specific for high energetic radiation, was used with the maximum opening angle. Using these conditions, the samples were measured between 3 and 35º (2θ) with a step size of 0.01º and with a total measurement time of 2 hours and 30 minutes. The samples were spun at 10 rpm.

In order to quantify the amorphous and non-diffracting content (ACn), the internal standard method was used [38]. Prior to LXRPD data collection, samples were mixed with ~20wt% of crystalline quartz. Samples were manually mixed with quartz in an agate mortar for 15 minutes and powder patterns were collected in the diffractometer. The hydration of the control samples was stopped prior to these measurements as detailed before. Contrarily, samples with MPCM were measured without stopping the hydration.

Additionally, *in situ* LXRPD experiments were performed in order to compare early age hydration development with the calorimetry results. Cement paste composites were mixed as previously described and introduced in two different Kapton film sample holders. The first round of measurements was done with one of the Kapton samples for the first 6 h. After this, a second round with the other Kapton sample was measured up to 10 h.

2.2.4. LXRPD data analysis

The patterns were analysed by the Rietveld method using a GSAS software package [39], utilizing a pseudo-Voight peak shape function with the asymmetry correction included [40, 41], to obtain Rietveld Quantitative Phase Analysis (RQPA). The refined parameters were: background coefficients, phase scale factors, unit cell parameters, zero-shift error and peak shape parameters.

2.2.5. Differential Scanning Calorimetry (DSC)

A differential scanning calorimeter METTLER TOLEDO model DSC 1 was used. The measurement cell is a silver furnace model 400 W which operates between room temperature and 700 ºC, with a heating speed maximum of 100 ºC/min, and a ceramic sensor model HSS8 formed by 120 thermopar of Au-Au/Pd. The device incorporates a liquid N_2 cooling system, which allows decreasing the temperature to -150 ºC. A continuous N_2 flux at 20 l/min was utilized as a protective gas. Samples are introduced in 40 µl Al crucible in a temperature range from -20 ºC to 60 ºC and back to -20 ºC at 3 ºC/min. Around 8-10 mg of sample was used. A calibration with In was done previous to the tests. The hydration of control samples was stopped prior to these measurements, as detailed before. Contrarily, samples with MPCM were measured without stopping the hydration.

2.2.6. Mercury intrusion porosimetry (MIP)

The pore size distribution was measured by MIP. Cylindrical samples (2.5 cm Φ x 1.5 cm height) of the cement composites were produced and cured until 28 days following the same procedure as for the compressive strength measurements described below. Before MIP measurements, the samples were dried at room temperature at 20% RH (relative humidity) until constant weight. Gently drying at room temperature is expected to avoid dehydration of cement hydrates and changes in the microstructure that might occur with oven drying [42-44]. Accordingly, even though there might be small deviations between the pore structure measured by MIP and the pores within the compressive strength samples, the results are expected to be comparable. These samples were crushed into smaller pieces to be measured by MIP. In order to measure porosity in the range from 1 mm down to 2 nm, a micromeritics AutoPore IV 9500 porosimeter (Micromeritics Instrument Corporation, Norcross - GA, US) was used. The pressure applied by the intrusion

porosimeter ranged from 0 to 200 MPa in step mode. A constant contact angle of 140° was assumed for data evaluation [45].

2.2.7. Compressive strength

Mortars were prepared according to UNE-EN196-1 at cement/sand and w/c mass ratios of 1/3 and 1/2, respectively. SP was utilized at a concentration of 2 wt% with respect to cement and MPCM, and CEN EN196-1 standard sand was used. Mortar cubes (3×3×3 cm^3) were cast and cured at 20±1 °C and 99% relative humidity (RH) for 24 h. The cubes were demolded and kept in a water bath (20±1 °C) until mechanical strength characterization (compression) was performed at 1, 7, 28 and 56 days. The reported value is the average of three measurements under the compression machine (Model Autotest 200/10 W, Ibertest, Madrid, Spain). The measured compressive strength values were corrected by the geometrical factor of 1.78 in order to obtain comparable values to those determined when using standard prisms (4x4x16 cm^3). This factor is obtained by dividing the compression area of the machine (1600 mm^2) with the area of the specimen (900 mm^2).

2.2.8. Scanning Electron Microscopy

The microstructure of the fracture surface of the cement composites, at 28 days of hydration, was observed through Scanning Electron Microscopy (SEM) (model Quanta 250, FEI Company) with a tungsten filament operating at a working potential of 15 kV.

3. RESULTS AND DISCUSSION

3.1 Phase assemblage of cement pastes

Table 4 shows the RQPA results of CSA control and CSA with MPCM pastes hydrated at t_0, 1, 7, 28 and 56 days at w/c of 0.5, including the amorphous (ACn) and free water (FW) contents. ACn

was determined by internal standard methodology as detailed in the experimental section. FW was calculated by analysing the DTA-TGA curves of stopped and non-stopped pastes [46], except for the t_0 columns, where the FW contents are the theoretical ones. The phase assemblage has not changed by inclusion of MPCM.

The degree of hydration of $C_4A_3\bar{S}$ in these pastes is given in Figure 2. The delay is noticeable only at 1 day of hydration, due to the presence of SP (see Section 3.3). When SP is added to CSA cement, there is a strong retardation of the early hydration of CSA cement, since the SP is mainly adsorbed on AFt [47-50]. At later stages, the degree of hydration of ye'elimite is even higher than that for the CSA control. This enhanced degree of reaction may be due to a better homogenization of the pastes due to the addition of SP, which increases the availability of water.

Table 4. Full phase assemblage[§] (RQPA, amorphous and free water) for CSA-control and CSA-D24 pastes at different ages at a w/c=0.5

	t_0	**t_0**	**1d**	**1d**	**7d**	**7d**	**28d**	**28d**	**56d**	**56d**
Phases	**CSA-control**	**CSA-D24**	**CSA-control**	**CSA-D24**	**CSA-control**	**CSA-D24**	**CSA-control**	**CSA-D24**	**CSA-control**	**CSA-D24**
$C_4A_3\bar{S}$	24.4	21.0	12.8	17.2	6.1	3.5	6.7	1.7	6.2	1.2
b-C_2S	9.6	6.7	12.0	6.6	11.0	7.2	11.2	5.1	11.4	4.6
CT	1.5	1.3	1.9	1.2	1.7	1.3	1.9	1.2	1.7	1.0
$C\bar{S}$	15.5	11.2	7.7	6.9	3.2	6.9	2.6	6.8	2.5	1.0
Akermanite	0.4	1.3	-	-	-	-	-	-	-	-
Mayenite	1.2	1.3	-	-	-	-	-	-	-	-
AFt	-	-	24.9	6.4	34.1	36.6	42.2	35.5	46.7	33.9
ACn	13.8	31.6	29.1	52.7	42.2	47.7	35.5	49.8	31.4	58.4
FW	33.3*	25.6*	11.6	8.9	1.8	1.4	0	0	0	0

* These values of FW are the total amount of added water, i.e., theoretical values.
§ The relative errors of the values are of the order of 2% for the main phases and increase to approximately 5-10% for the low-content components [51].

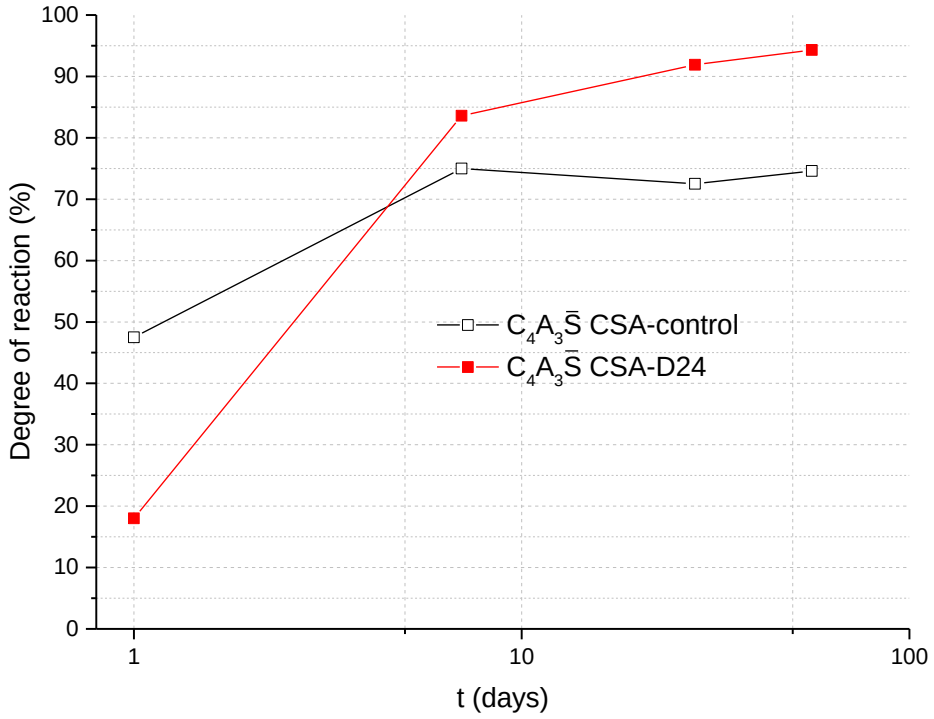

Figure 2. Degree of reaction of $C_4A_3\bar{S}$ as a function of time

3.2 Isothermal Calorimetry

Figure 3a shows the calorimetric curves (heat flow and total cumulated heat) for CSA pastes at w/c of 0.5 during 7 days of hydration. Before ~10 h of hydration, three peaks are observed for the CSA-control, which has been attributed to ettringite formation at short hydration times [49]. The second peak at ~35 h has been attributed to hydration of the remaining ye'elimite after total depletion of anhydrite, leading to formation of monosulphate [49].

CSA-D24 exhibits a strong retardation and the calorimetric curves are significantly different from the CSA-control. As will be discussed in the next section, this retardation in CSA is due to SP addition. The three first signals (ettringite formation) appear much more separated in time. In addition, the last signal has the highest intensity, while it has the lowest intensity for CSA-control. It is possible that for CSA-D24 the sulphate depletion peak overlaps with the last peak for ettringite formation. The total heat released after 7 days of hydration for CSA-D24 (347 J/g) is also similar

than that of CSA-control (327 J/g). The time of hydration when CSA-D24 achieves the same cumulative heat as CSA-control is ~62 hours.

In order to compare the samples, a sample of CSA with 2 wt% of SP and w/c=0.34 was measured (in green). This w/c was chosen as the sample with MPCM has w/c=0.5, meaning that the w/s (water/solids) is 0.34, taking into account the 45 wt% of MPCM. The hydration of CSA is significantly delayed in the similar way as the CSA-D24 sample, confirming that the delay is mainly due to SP.

The delay of the early hydration of CSA cement, corresponding to a delay in the early formation of AFt crystals [52, 53] has also been observed by LXRPD. Figure 3b provides the AFt and ye'elimite contents determined by Rietveld method, during the first 10 h of hydration. It is clearly observed that the reaction of ye'elimite to form ettringite is strongly inhibited in the sample with MPCM, in agreement with the heat released by this sample. It is assumed that SP is adsorbed onto the surface of the clinker particles, thereby suppressing ettringite formation [54].

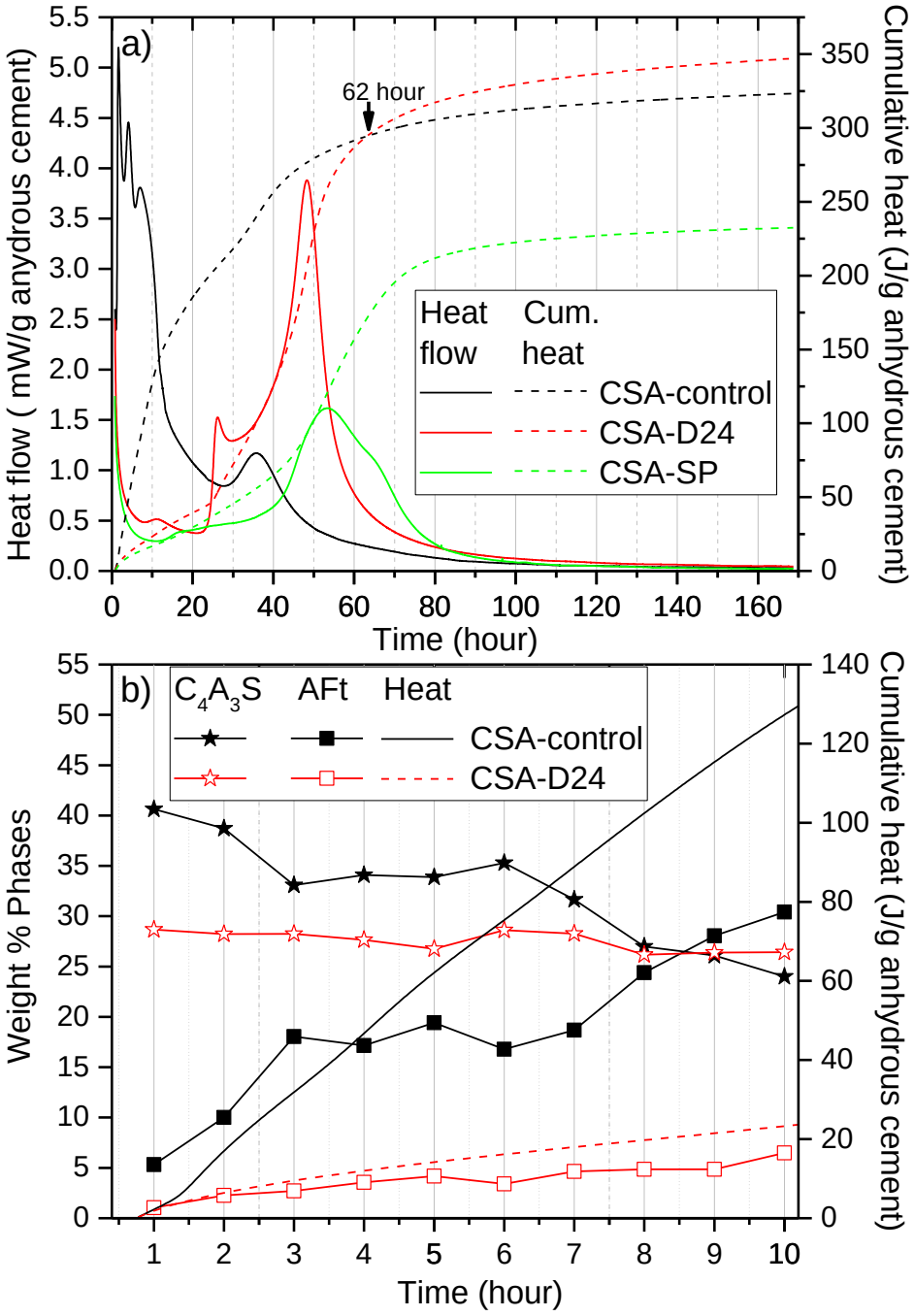

Figure 3. (a) Calorimetric curves during the first 7 days for CSA-control, CSA-D24, and CSA-SP. (b) Ettringite (squares) and ye'elimite (stars) contents, determined by in-situ RQPA and cumulative heat during the first 10 hours of hydration of both samples.

3.3 Delaying effect of SP

In order to confirm that the retarding effect was only due to SP, as previously claimed by Wei et al. [21] and She et al. [55], and to gain a better understanding of the different signals observed

256 in the calorimetric curves, tests without SP were performed. In order to prepare samples with
257 usable workability, a much higher w/c ratio (0.75) was needed in the absence of SP. Samples
258 without and with MPCM were compared.

259 Figure 4 shows heat flow for CSA without and with MPCM at w/c of 0.75 for up to 3 days of
260 hydration. The curves of the samples with and without MPCM are almost coincident, illustrating
261 that the retarding effect is not due to MPCM addition.

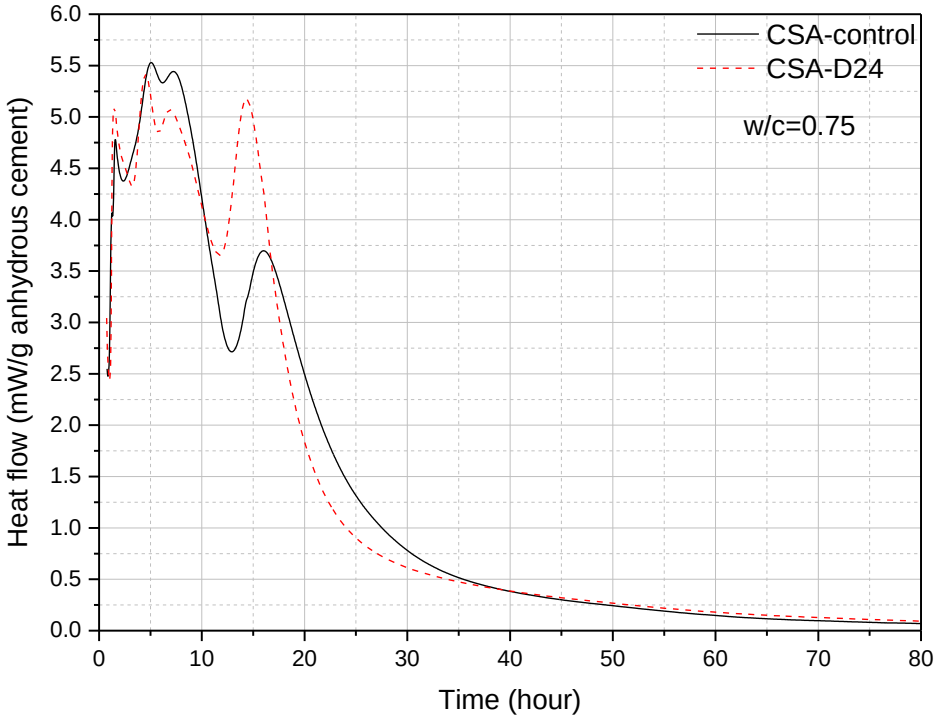

262
263 *Figure 4. Heat flow curves for CSA pastes with w/c=0.75 for up to 3 days of hydration*
264

265 The sulphate depletion peak is significantly different for the MPCM sample compared to the
266 control. Accordingly, at early ages (less 24 h) the kinetics are different when MPCM is present in
267 the system, probably due to the filler effect [56] of MPCM. However, the final performance of the
268 composites with MPCM is not negatively affected.

3.4 Thermal study by DSC

Figure 5 shows the heating (from -20 to 60ºC) DSC curves of CSA pastes at different curing ages and Table 5 provides the heat data. The enthalpy of fusion measured with respect to the pure MPCM is also given in Table 5.

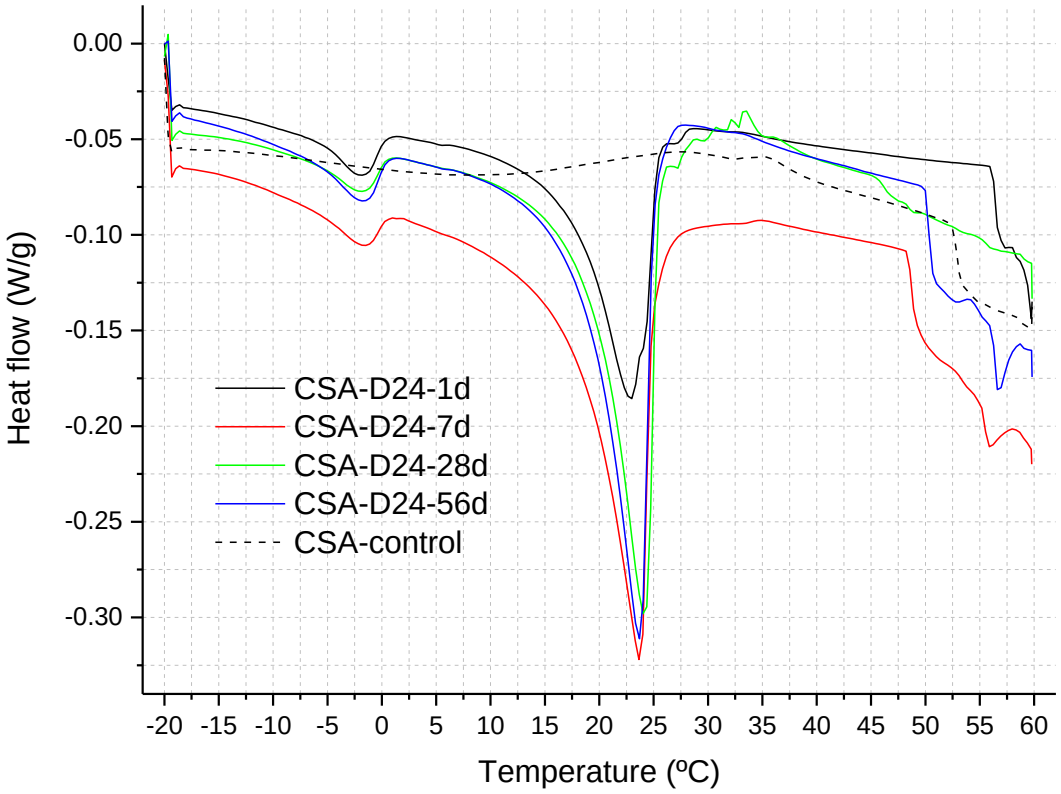

Figure 5. DSC curves for the indicated samples

Except at 1 day, the values are close to the theoretical values predicted from the mass percentage of MPCM in the cement composites (22.7 %). The thermal behaviour of MPCM is not affected by the cement matrix with time, since the onset, endset and peak temperature are almost constant (Table 5). This means that the functionality of the MPCM is not altered by the process of cement hydration, which suggests that the MPCM has withstood the mixing process.

Table 5. Thermal data obtained for the studied samples

Designation	Weight of sample (mg)	Melting				
		Onset (ºC)	Endset (ºC)	Absolute Enthalpy (J/g)	Relative Enthalpy (%)	Peak T (ºC)
Pure MPCM	3.0	16.6	26.6	119.1	100	23.7
CSA D24-1d	10.6	17.0	25.3	17.2	14.4	22.9
CSA D24-7d	10.8	17.6	24.9	28.2	23.7	23.7
CSA D24-28d	9.5	19.0	25.4	25.4	21.3	24.1
CSA D24-56d	7.3	18.3	25.0	25.4	21.3	23.7

3.5 Mercury Intrusion Porosimetry of cement pastes

Figure 6 gives the MIP results for both samples. The total porosity determined by this method is similar in the presence of MPCM (18.4%) and for the control sample (20.9%). It should be noted that SP can act as a defflocculant agent, taking air out. The total porosity of the MPCM sample is slightly smaller and the hydration degree of this sample is higher than that of the control sample, as evidenced by the XRD and Isothermal calorimetry results. Although the total porosity is not higher in the presence of MPCM, the sizes of the pores are higher, see Figure 6. This suggests that the samples with MPCM will develop lower mechanical strengths.

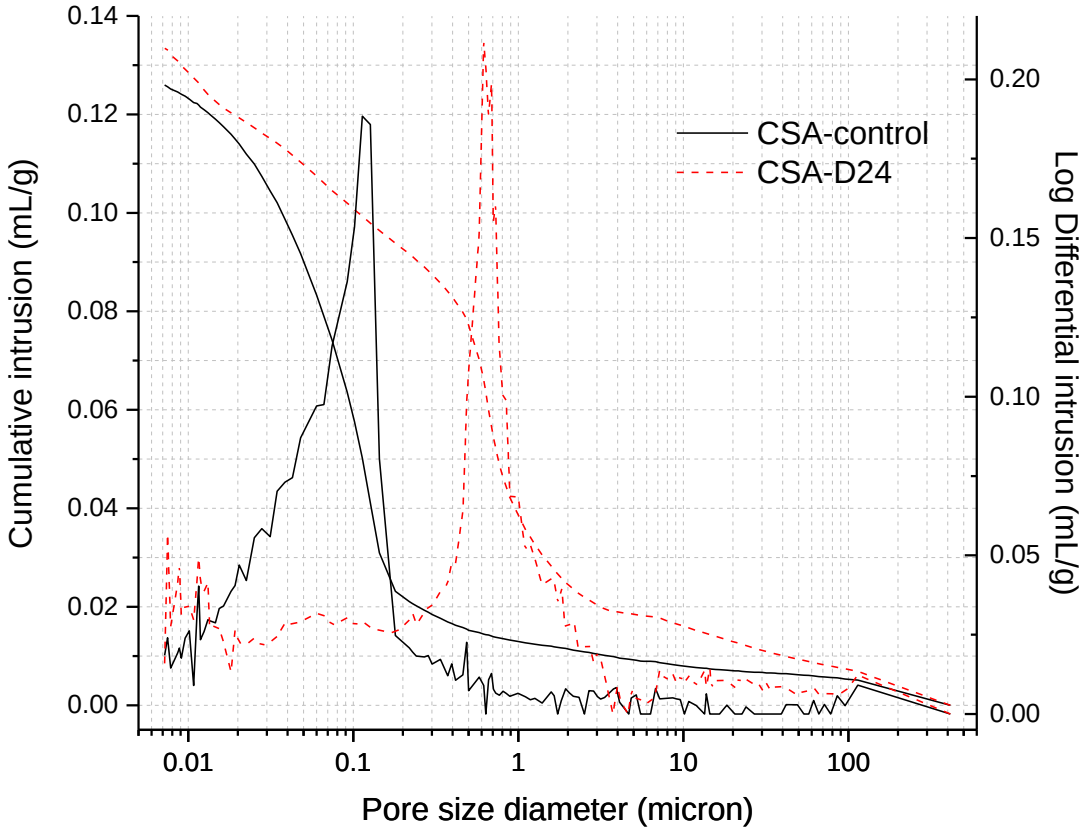

Figure 6. Cumulative intrusion curve and pore size distribution for samples at 28 days.

3.6 Compressive strength

Compressive strengths of the mortar composites are given in Figure 7. The addition of MPCM provokes a dramatic decrease of the mechanical strengths at all ages. This may be a physical effect due to i) the low resistance of the organic shell of the MPCM and ii) the absence of interactions between the MPCM and the cement matrix (Figure 8). Figure 8 gives a SEM image of a cement paste sample at 28 days. There is little interaction between the MPCM particles and the cement matrix. In some cases, a gap between the particles and the cement matrix is clearly observed. The lack of interactions in the interfacial zone may provoke a reduction of the compressive strengths [19]. Moreover, the MPCM particles remains unbroken, illustrating that they are strong enough to withstand the mixing process without breaking**,** as reported in Sanfelix et al. [28].

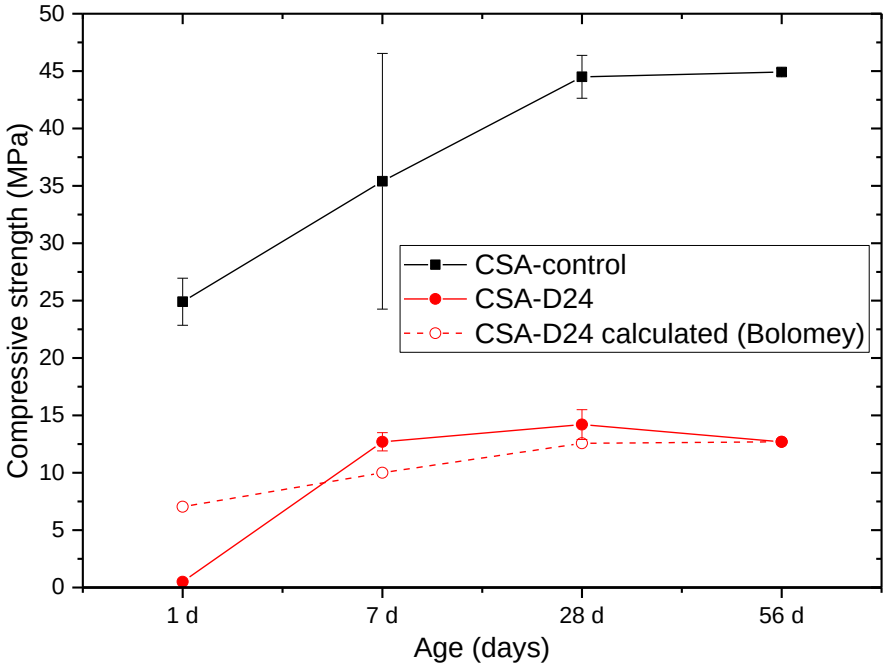

Figure 7. Compressive strengths of CSA mortars, prepared at w/c=0.50 with and without MPCM and 2.0 wt% SP. Calculated strengths from the Bolomey equation considering the volume of MPCM as air (open symbols)

The dramatic decrease of mechanical strengths could also be attributed to the lower volume percentage of cement which is present in CSA-D24 (13 vol%) compared to the control sample (42 vol%), i.e., about 60 vol % reduction of cement content in the sample with MPCM.

Since the microcapsules could have a similar effect on the compressive strength as air voids, it is interesting to utilize the Bolomey equation [57, 58] to predict the compressive strengths considering the MPCM volume as air voids:

$$f_c = K_B \times \sigma_C \left[\frac{C}{W + W_v + W_{MPCM}} - 0.5 \right]$$

where f_c is the calculated compressive strength, K_B is a constant depending on the utilized aggregates, σ_C is dependent on the cement class, C is the mass of cement in the mix, W is the mass of water, W_V is the mass of water equivalent to the volume of entrapped air voids, and W_{MPCM} is the mass of water equivalent to the volume of MPCM. Since K_B and σ_C are the same for both

samples, the reduction in compressive strength of the sample containing MPCM can be calculated from the contents of the different components in each sample together with the air content from the MIP experiments (section 3.5). As can be seen from the open symbols in Figure 7, the calculated strengths for CSA-D24 are very close to the experimental ones. This confirms that the compressive strength reduction is mainly due to air pores and addition of MPCM, and that the effect of MPCM is very similar to that of air voids inside the mortar. While the experimental and calculated values are very similar at long curing times, after only 1 day of curing the value calculated from the Bolomey equation is significantly higher than the measured value. This is probably caused by the slower reaction rate of the samples containing MPCM (due to the SP-addition), as is evident from Figure 3a.

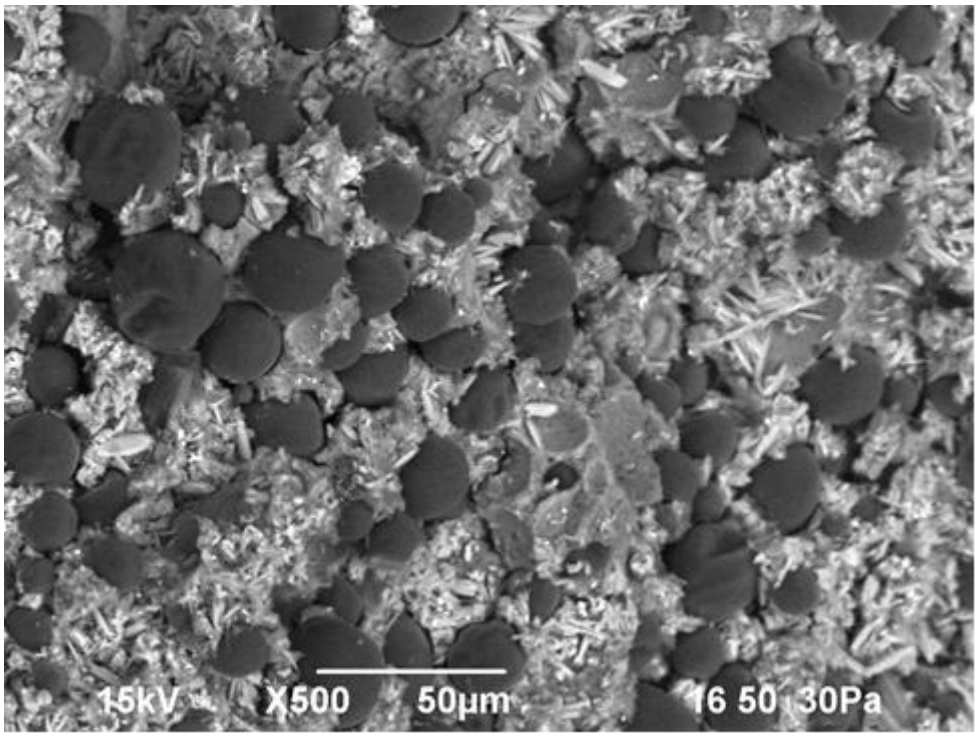

Figure 8. SEM image of a freshly fractured sample of CSA-D24 at 28 days

4. CONCLUSIONS

This study has been focused in the development of CSA cement mixed with MPCM incorporating superplasticizer in the composites in order to improve workability. The MPCM content was the highest possible [28], in order to get the maximum efficiency with regards to the thermal properties. The mechanism of hydration of CSA is not affected by the addition of MPCM, since the phase assemblage is the same at all studied hydration ages. Due to the presence of SP in the composite matrix, there is a possible interference between the effects of MPCM and SP addition on the cement. However, it has been shown that the addition of MPCM did not affect the kinetics of CSA hydration. The DSC results demonstrated that the introduced MPCM is stable in the composites considering the latent heat content. Although neither the hydration mechanisms nor the total porosity have changed due to the addition of MPCM, there is a dramatic decrease of the compressive strength. This is caused by i) the fact of MPCM is acting similar to air bubbles in the mortar and ii) the very low cohesive force between MPCM and cement matrix. The compressive strength reduction at long curing times is in very good agreement with the Bolomey equation, if MPCM is considered to have the same effect as air voids.

Acknowledgements

We gratefully acknowledge funding from the Research Council of Norway, project number 238198. The authors gratefully acknowledge PhD. Luis Miguel Ordoñez at Kheme Chemical S.L. and Eng. Rino Nilsen at Østfold University College for technical assistance.

353

354 **REFERENCES**

355 [1] E. Gartner, Industrially interesting approaches to “low-CO2” cements, Cement and Concrete
356 Research, 34 (2004) 1489-1498.

357 [2] M.A.G. Aranda, A.G. De la Torre, 18 - Sulfoaluminate cement, in: F. Pacheco-Torgal, S.
358 Jalali, J. Labrincha, V.M. John (Eds.) Eco-Efficient Concrete, Woodhead Publishing2013, pp.
359 488-522.

360 [3] F. Winnefeld, B. Lothenbach, Phase equilibria in the system Ca4Al6O12SO4 – Ca2SiO4 –
361 CaSO4 – H2O referring to the hydration of calcium sulfoaluminate cements, RILEM Technical
362 Letters, 1 (2016) 10.

363 [4] F. Winnefeld, B. Lothenbach, Hydration of calcium sulfoaluminate cements — Experimental
364 findings and thermodynamic modelling, Cement and Concrete Research, 40 (2010) 1239-1247.

365 [5] F. Winnefeld, S. Barlag, Calorimetric and thermogravimetric study on the influence of
366 calcium sulfate on the hydration of ye’elimite, Journal of Thermal Analysis and Calorimetry, 101
367 (2010) 949-957.

368 [6] A. Telesca, M. Marroccoli, M.L. Pace, M. Tomasulo, G.L. Valenti, P.J.M. Monteiro, A
369 hydration study of various calcium sulfoaluminate cements, Cement and Concrete Composites,
370 53 (2014) 224-232.

371 [7] M. García-Maté, A.G. De la Torre, L. León-Reina, E.R. Losilla, M.A.G. Aranda, I.
372 Santacruz, Effect of calcium sulfate source on the hydration of calcium sulfoaluminate eco-
373 cement, Cement and Concrete Composites, 55 (2015) 53-61.

374 [8] K. Ndiaye, M. Cyr, S. Ginestet, Durability and stability of an ettringite-based material for
375 thermal energy storage at low temperature, Cement and Concrete Research, 99 (2017) 106-115.

[9] K. Ndiaye, S. Ginestet, M. Cyr, Experimental evaluation of two low temperature energy storage prototypes based on innovative cementitious material, Applied Energy, 217 (2018) 47-55.

[10] J. Kaufmann, F. Winnefeld, Seasonal heat storage in calcium sulfoaluminate based hardened cement pastes – experiences with different prototypes, Journal of Energy Storage, 25 (2019) 100850.

[11] V.D. Cao, S. Pilehvar, C. Salas-Bringas, A.M. Szczotok, T.Q. Bui, M. Carmona, J.F. Rodriguez, A.-L. Kjøniksen, Thermal performance and numerical simulation of geopolymer concrete containing different types of thermoregulating materials for passive building applications, Energy and Buildings, 173 (2018) 678-688.

[12] V.D. Cao, S. Pilehvar, C. Salas-Bringas, A.M. Szczotok, T.Q. Bui, M. Carmona, J.F. Rodriguez, A.-L. Kjøniksen, Thermal analysis of geopolymer concrete walls containing microencapsulated phase change materials for building applications, Solar Energy, 178 (2019) 295-307.

[13] V.D. Cao, T.Q. Bui, A.-L. Kjøniksen, Thermal analysis of multi-layer walls containing geopolymer concrete and phase change materials for building applications, Energy, 186 (2019) 115792.

[14] U. Berardi, A.A. Gallardo, Properties of concretes enhanced with phase change materials for building applications, Energy and Buildings, 199 (2019) 402-414.

[15] S.E. Kalnæs, B.P. Jelle, Phase change materials and products for building applications: A state-of-the-art review and future research opportunities, Energy and Buildings, 94 (2015) 150-176.

[16] J. Pereira da Cunha, P. Eames, Thermal energy storage for low and medium temperature applications using phase change materials – A review, Applied Energy, 177 (2016) 227-238.

[17] A. Karaipekli, A. Sarı, Development and thermal performance of pumice/organic PCM/gypsum composite plasters for thermal energy storage in buildings, Solar Energy Materials and Solar Cells, 149 (2016) 19-28.

[18] S. Pilehvar, V.D. Cao, A.M. Szczotok, M. Carmona, L. Valentini, M. Lanzón, R. Pamies, A.-L. Kjøniksen, Physical and mechanical properties of fly ash and slag geopolymer concrete containing different types of micro-encapsulated phase change materials, Construction and Building Materials, 173 (2018) 28-39.

[19] S. Pilehvar, V.D. Cao, A.M. Szczotok, L. Valentini, D. Salvioni, M. Magistri, R. Pamies, A.-L. Kjøniksen, Mechanical properties and microscale changes of geopolymer concrete and Portland cement concrete containing micro-encapsulated phase change materials, Cement and Concrete Research, 100 (2017) 341-349.

[20] S. Pilehvar, A.M. Szczotok, J.F. Rodríguez, L. Valentini, M. Lanzón, R. Pamies, A.-L. Kjøniksen, Effect of freeze-thaw cycles on the mechanical behavior of geopolymer concrete and Portland cement concrete containing micro-encapsulated phase change materials, Construction and Building Materials, 200 (2019) 94-103.

[21] Z. Wei, G. Falzone, B. Wang, A. Thiele, G. Puerta-Falla, L. Pilon, N. Neithalath, G. Sant, The durability of cementitious composites containing microencapsulated phase change materials, Cement and Concrete Composites, 81 (2017) 66-76.

[22] M. Frigione, M. Lettieri, A. Sarcinella, Phase Change Materials for Energy Efficiency in Buildings and Their Use in Mortars, Materials (Basel, Switzerland), 12 (2019) 1260.

[23] A. Maldonado-Alameda, A.M. Lacasta, J. Giro-Paloma, J.M. Chimenos, L. Haurie, J. Formosa, Magnesium phosphate cements formulated with low grade magnesium oxide incorporating phase change materials for thermal energy storage, Construction and Building Materials, 155 (2017) 209-216.

[24] G. Sang, Y. Cao, M. Fan, G. Lu, Y. Zhu, Q. Zhao, X. Cui, Development of a novel sulphoalumitate cement-based composite combing fine steel fibers and phase change materials for thermal energy storage, Energy and Buildings, 183 (2019) 75-85.

[25] A. Eddhahak, S. Drissi, J. Colin, S. Caré, J. Neji, Effect of phase change materials on the hydration reaction and kinetic of PCM-mortars, Journal of Thermal Analysis and Calorimetry, 117 (2014) 537-545.

[26] P. Meshgin, Y. Xi, Y. Li, Utilization of phase change materials and rubber particles to improve thermal and mechanical properties of mortar, Construction and Building Materials, 28 (2012) 713-721.

[27] A.M. Thiele, Z. Wei, G. Falzone, B.A. Young, N. Neithalath, G. Sant, L. Pilon, Figure of merit for the thermal performance of cementitious composites containing phase change materials, Cement and Concrete Composites, 65 (2016) 214-226.

[28] S.G. Sanfelix, I. Santacruz, A.M. Szczotok, L.M.O. Belloc, A.G. De la Torre, A.-L. Kjøniksen, Effect of microencapsulated phase change materials on the flow behavior of cement composites, Construction and Building Materials, 202 (2019) 353-362.

[29] G. Álvarez-Pinazo, I. Santacruz, M.A.G. Aranda, Á.G.D.l. Torre, Hydration of belite–ye'elimite–ferrite cements with different calcium sulfate sources, Advances in Cement Research, 28 (2016) 529-543.

442 [30] G. Álvarez-Pinazo, A. Cuesta, M. García-Maté, I. Santacruz, E.R. Losilla, A.G.D. la Torre,
443 L. León-Reina, M.A.G. Aranda, Rietveld quantitative phase analysis of Yeelimite-containing
444 cements, Cement and Concrete Research, 42 (2012) 960-971.
445 [31] D. Gastaldi, G. Paul, L. Marchese, S. Irico, E. Boccaleri, S. Mutke, L. Buzzi, F. Canonico,
446 Hydration products in sulfoaluminate cements: Evaluation of amorphous phases by XRD/solid-
447 state NMR, Cement and Concrete Research, 90 (2016) 162-173.
448 [32] A.G. De la Torre, I. Santacruz, L. León-Reina, A. Cuesta, M.A.G. Aranda, Diffraction and
449 crystallography applied to anhydrous cements, Cementitious Materials: Composition, Properties,
450 Application, 2017.
451 [33] M.A.G. Aranda, A. Cuesta, A.G. De la Torre, I. Santacruz, L. León-Reina, 2. Diffraction
452 and crystallography applied to hydrating cements, Cementitious Materials: Composition,
453 Properties, Application, 2017.
454 [34] M. García-Maté, I. Santacruz, A.G. De la Torre, L. León-Reina, M.A.G. Aranda,
455 Rheological and hydration characterization of calcium sulfoaluminate cement pastes, Cement
456 and Concrete Composites, 34 (2012) 684-691.
457 [35] P.-C. Aitcin, C. Jolicoeur, J.G. MacGregor, Superplasticizers: how they work and why they
458 occasionally don't, Concrete International, 16 (1994) 45-52.
459 [36] M. García-Maté, A.G. De la Torre, L. León-Reina, M.A.G. Aranda, I. Santacruz, Hydration
460 studies of calcium sulfoaluminate cements blended with fly ash, Cement and Concrete Research,
461 54 (2013) 12-20.
462 [37] L. Wadsö, Operational issues in isothermal calorimetry, Cement and Concrete Research, 40
463 (2010) 1129-1137.

[38] A.G. De La Torre, S. Bruque, M.A.G. Aranda, Rietveld quantitative amorphous content analysis, Journal of Applied Crystallography, 34 (2001) 196-202.

[39] A.C. Larson, R.B. Von Dreele, Gsas, Report lAUR, (1994) 86-748.

[40] P. Thompson, D.E. Cox, J.B. Hastings, Rietveld refinement of Debye-Scherrer synchrotron X-ray data from Al2O3, Journal of Applied Crystallography, 20 (1987) 79-83.

[41] L.W. Finger, D.E. Cox, A.P. Jephcoat, A correction for powder diffraction peak asymmetry due to axial divergence, Journal of Applied Crystallography, 27 (1994) 892-900.

[42] A. Korpa, R. Trettin, The influence of different drying methods on cement paste microstructures as reflected by gas adsorption: Comparison between freeze-drying (F-drying), D-drying, P-drying and oven-drying methods, Cement and Concrete Research, 36 (2006) 634-649.

[43] C. Gallé, Effect of drying on cement-based materials pore structure as identified by mercury intrusion porosimetry: A comparative study between oven-, vacuum-, and freeze-drying, Cement and Concrete Research, 31 (2001) 1467-1477.

[44] M. Moukwa, P.C. Aïtcin, The effect of drying on cement pastes pore structure as determined by mercury porosimetry, Cement and Concrete Research, 18 (1988) 745-752.

[45] H. Ma, Mercury intrusion porosimetry in concrete technology: Tips in measurement, pore structure parameter acquisition and application, 2014.

[46] J.D. Zea-Garcia, I. Santacruz, M.A.G. Aranda, A.G. De la Torre, Alite-belite-ye'elimite cements: Effect of dopants on the clinker phase composition and properties, Cement and Concrete Research, 115 (2019) 192-202.

[47] N. Sun, W. Chang, L. Wang, J. Zhang, M. Pei, Effects of the Chemical Structure of Polycarboxy-Ether Superplasticizer on Its Performance in Sulphoaluminate Cement, Journal of Dispersion Science and Technology, 32 (2011) 795-798.

[48] J. Plank, C. Hirsch, Impact of zeta potential of early cement hydration phases on superplasticizer adsorption, Cement and Concrete Research, 37 (2007) 537-542.

[49] F. Winnefeld, Interaction of superplasticizers with calcium sulfoaluminate cements, Tenth International Conference on Superplasticizers and Other Chemical Admixtures in ConcretePrague, Czech Republic, 2012, pp. 21-36.

[50] R. Belhadi, A. Govin, P. Grosseau, Hydration and rheology of sulfoaluminate cements (CSA) in presence of polycarboxylate superplasticizers (PCE) and citric acid, 15th International Congress on the Chemistry of Cement a success (ICCC 2019), Research Institute of Binding Materials Prague Ltd., Prague, Czech Republic, 2019, pp. ID 165.

[51] A.G. De la Torre, M.A.G. Aranda, Accuracy in Rietveld quantitative phase analysis of Portland cements, Journal of Applied Crystallography, 36 (2003) 1169-1176.

[52] T. Su, X. Kong, H. Tian, D. Wang, Effects of comb-like PCE and linear copolymers on workability and early hydration of a calcium sulfoaluminate belite cement, Cement and Concrete Research, 123 (2019) 105801.

[53] M.R. Meier, A. Rinkenburger, J. Plank, Impact of different types of polycarboxylate superplasticisers on spontaneous crystallisation of ettringite, Advances in Cement Research, 28 (2016) 310-319.

[54] H. Tian, X. Kong, Y. Cui, Q. Wang, D. Wang, Effects of polycarboxylate superplasticizers on fluidity and early hydration in sulfoaluminate cement system, Construction and Building Materials, 228 (2019) 116711.

[55] Z. She, Z. Wei, B.A. Young, G. Falzone, N. Neithalath, G. Sant, L. Pilon, Examining the effects of microencapsulated phase change materials on early-age temperature evolutions in realistic pavement geometries, Cement and Concrete Composites, 103 (2019) 149-159.

510 [56] G.C. Cordeiro, R.D. Toledo Filho, L.M. Tavares, E.M.R. Fairbairn, Pozzolanic activity and
511 filler effect of sugar cane bagasse ash in Portland cement and lime mortars, Cement and Concrete
512 Composites, 30 (2008) 410-418.
513 [57] T. Lecompte, P. Le Bideau, P. Glouannec, D. Nortershauser, S. Le Masson, Mechanical and
514 thermo-physical behaviour of concretes and mortars containing phase change material, Energy
515 and Buildings, 94 (2015) 52-60.
516 [58] J. Bolomey, Determination of the compressive strength of mortars and concretes, Bull Tech
517 Suisse Romande, 16 (1927) 22-24.
518